

Study on axial compressive behavior of quadruple C-channel built-up cold-formed steel columns

Shaofeng Nie^{*1}, Tianhua Zhou^{1a}, Fangfang Liao¹ and Donghua Yang²

¹School of Civil Engineering, Chang'an University, Xi'an, 710061, China

²China West Airport Group, Xi'an, 710075, China

(Received December 4, 2017, Revised September 20, 2018, Accepted March 5, 2019)

Abstract. In this study, the axial compressive behavior of novel quadruple C-channel built-up cold-formed steel columns with different slenderness ratio was investigated, using the experimental and numerical analysis. The axial compressive capacity and failure modes of the columns were obtained and analyzed. The finite element models considering the geometry, material and contact nonlinearity were developed to simulate and analyze the structural behavior of the columns further. There was a great correlation between the numerical analyses and test results, which indicated that the finite element model was reasonable and accurate. Then influence of, slenderness ratio, flange width-to-thickness ratio and screw spacing on the mechanical behavior of the columns were studied, respectively. The tests and numerical results show that due to small slenderness ratio, the failure modes of the specimens are generally local buckling and distortional buckling. The axial compressive strength and stiffness of the quadruple C-channel built-up cold-formed steel columns decrease with the increase of maximum slenderness ratio. When the screw spacing is ranging from 150mm to 450mm, the axial compressive strength and stiffness of the quadruple C-channel built-up cold-formed steel columns change little. The axial compressive capacity of quadruple C-channel built-up cold-formed steel columns increases with the decrease of flange width-thickness ratio. A modified effective length factor is proposed to quantify the axial compressive capacity of the quadruple C-channel built-up cold-formed steel columns with U-shaped track in the ends.

Keywords: cold-formed steel; built-up section; compressive tests; numerical analysis; axial compressive capacity; effective ratio of width-to-thickness method; direct strength method

1. Introduction

Cold-formed steel structures have been widely developed and used in the field of structural engineering in recent years, due to its superior strength-to-weight ratio capacity and ease of construction. Complex built-up cold-formed members, which are generally composed of C-shaped and U-shaped components, connected by self-drilling screws, are typical main load-bearing elements for construction in such a structural system. These types of complex cold-formed members are generally employed in window framing, doorways, shear walls and other core parts where need to be strengthened (Yu 2000). Therefore, the structural behavior of these complex cold-formed member types should be fully understood.

Many researches on the behavior of cold-formed steel column with single channel were carried out through experimental and finite element method (FEM). Dong (2006) studied the hysteretic behaviors of channel and C-section cold-formed steel members under cyclic axial loading with the finite element method. The performance and strengths of cold-formed steel non-symmetric lipped

angle columns were investigated by Young and Chen (2008). Kripka and Pravia (2013) carried out a numerical study aimed at minimizing the weight of lipped and unlipped cold-formed channel columns, following the AISI 2007 specification. Flexural, torsional and torsional-flexural buckling of columns was considered as constraints. Muthuraj *et al.* (2017) reported the numerical investigation conducted to study the influence of Local-Distortional (L-D) interaction mode buckling on post buckling strength erosion in fixed ended lipped channel cold-formed steel columns.

Review of the state-of-the-art shows that some researches have been conducted to investigate the structural behavior of the cold-formed built-up members. Peters (2003) investigated on double-limb built-up columns made of C-shaped and U-shaped members. This study showed that the compressive capacity of the built-up column was greatly affected by the fastener spacing. Further, Stone and Laboube (2005) studied the axial compressive behaviors of the I-section column composed of two C-shaped members. It was shown by Whittle and Ramseyer (2009) that the modified slenderness ratio method in AISI was conservative in calculating axial compressive capacity of double-limb closed-box section built-up columns. Eight full-scale column tests were performed to study the overall compressive capacity of double-Z columns by Georgieva *et al.* (2012). After a series of analyses, the authors proposed some amendments in Standard Eurocode 3 (2006), as well

*Corresponding author, Associate Professor, Ph.D.

E-mail: niesf126@126.com

^a Professor, Ph.D.

E-mail: zhouth163@163.com

as in design approach which was based on the direct strength method. The influence of stiffener ties and spacers on the behavior and ultimate capacity of intermediate length CFS open section columns under axial compression was investigated by (Anbarasu *et al.* 2013, 2014). The results showed that the depth and number of spacers had significant influence on the behavior and strength of the columns. An axial load capacity equation for doubly symmetric built-up cold-formed sections with enough intermediate, symmetrical connections were developed by Piyawat *et al.* (2013). In the study, a numerical parametric study was conducted on a total of 360 different configurations and compared with the AISI specification and previous experimental data. Based on the analyses and comparisons, the axial load capacities for doubly symmetric built-up cold-formed tubular and I sections were evaluated. Li *et al.* (2014) studied the ultimate load-carrying capacity of the built-up box and I section columns through experimental investigation and numerical analysis. The behavior of cold-formed steel built-up open section columns with edge and web stiffeners under axial compression were numerically investigated by Zhang and Young (2015). Dabaon and Ellobody (2015) studied the built-up cold-formed steel section battened columns. Experimental testing of built-up members was conducted by Biggs *et al.* (2015), and the results showed that AISI-2001 and AISI-2007 were found to give inconsistent results that at times were un-conservative or overly conservative in terms of axial strength. Apart from the researches mentioned above, some practical methods have been also proposed in some structural specification to calculate the load capacity of the built-up cold-formed members, e.g. an equivalent modified slenderness ratio method has been provided in the AISI (2007) and Australia standard (AS/NZS No.4600 2005) to calculate the axial compressive capacity of double-limb built-up columns.

The current design method in Chinese code “Technical code of cold-formed thin-walled steel structures” (GB50018 2002) only includes the design rules for simple built-up members. On the other hand, limited test datum are available on calculating method for the compressive capacity of complex section cold-formed thin-walled built-up columns. Compared with individual cold-formed steel columns (Dong 2006, Young and Chen 2008, Heva and Mahendran 2013, Muthuraj *et al.* 2017, Zhou and Jiang 2017), the behavior and design of the complex built-up cold-formed steel columns are more complicated. Therefore, further studies were needed to widen the utilization of such built-up section members. In this condition, a novel complex cold-formed steel built-up column, namely quadruple C-channel built-up cold-formed steel column, is proposed and investigated in this study.

In this paper, a total of eight quadruple C-channel built-up cold-formed steel columns with different slenderness ratios were tested under axial compression. The tests would compensate the lack of experimental data on this form for construction and would provide the available experimental data for the further numerical study. Here the failure modes and strength of the columns were analyzed. The load-displacement and load-strain curves were measured in the tests. The parametric analyses, which investigated the

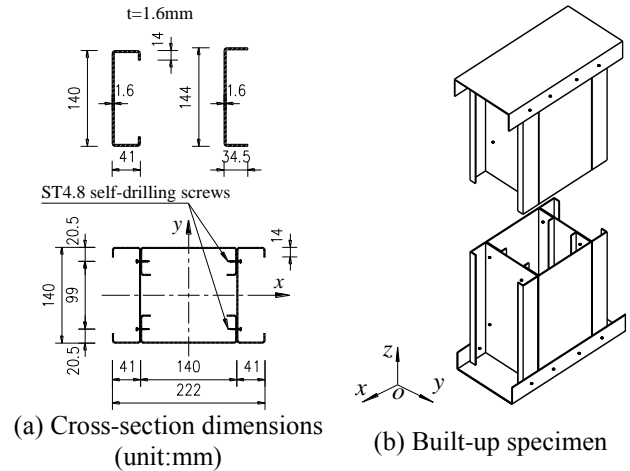


Fig. 1 Cross section dimensions and investigated built-up specimen

slenderness ratio, screw spacing and the flange width-to-thickness ratio on the mechanical behavior of quadruple C-channel built-up cold-formed steel columns under axial compression, were carried out based on the verified numerical models.

2. Compressive tests

2.1 Test specimens

Eight quadruple C-channel built-up cold-formed steel columns were tested in this study. The cross-section dimensions of the quadruple C-channel built-up cold-formed steel columns being investigated is shown in Fig. 1(a). The test specimen is formed by 4 C-shaped components with 2 U-shaped tracks connected at both ends of the members by using the ST4.8 self-drilling screws (see Fig. 1(b)). According to the length of the built-up column, test specimens can be divided into three length types: LC (long column), MC (intermediate length column) and SC (short column) types whose lengths are 3000mm, 1200mm and 450mm, respectively. The screws were set in the longitudinal direction of the specimens with a varying spacing of 300mm for MC and LC type specimens and 150mm for SC type specimens. Meanwhile, reinforced connections were located 100mm away from the both ends of MC and LC type specimens.

2.2 Material properties

The cold-formed plate used for the columns in this study is the Chinese Q235B grade steel plate with a zinc-aluminum galvanized layer. The nominal thickness of the steel plates was 1.5mm. In the test, the material properties of the specimens were obtained through three standard tensile coupon tests according to the Chinese Standard (GB/T228.1 2010). The measured material properties are summarized in Table 1.

2.3 Initial imperfections and residual stresses

The initial deflection of each C-shaped component on the test columns was measured. It was shown in the



(a) For LC type



(b) For MC, SC type

Fig. 2 Test set-up for built-up specimens

Table 1 Measured material properties obtained from tensile coupon tests

Specimen number	Thickness (mm)	Yield stress (MPa)	Ultimate stress (MPa)	Elastic modulus $\times 10^5$ (MPa)	Percentage elongation after fracture (%)
P161	1.54	341.02	451.53	2.22	32.81
P162	1.58	328.63	438.16	2.24	27.43
P163	1.56	332.46	444.51	2.23	32.81

measurement that the average value of the initial deflection at mid-span of each C-shaped component on each test column can basically be controlled to be lower than 3mm, which is relatively low compared with the length of the column. In the meantime, it is generally accepted that the residual stress on the cold-formed steel is relatively low (e.g. 7% of the yield strength of the steel (Young and Rasmussen 1998)) with a positive effect to counteract the increase of the whole section strength resulted by the increase of the yield strength and tensile stress in the angle of the section in the cold forming process. Thus, the effect of the residual stresses on the compressive capacity of the cold-formed thin-walled steel stub columns could be ignored in this study.

2.4 Test set-up

The axial compressive tests were conducted on the investigated quadruple C-channel built-up cold-formed steel columns. According to the length of the specimens, different test set-ups were used to apply the vertical compressive load on the different types of specimens being assessed, where the hydraulic jack was used for LC type specimens (see Fig. 2(a)) whereas the YE-2000A hydraulic compression-testing machine was used for MC and SC type specimens (see Fig. 2(b)). In the test, the built-up columns

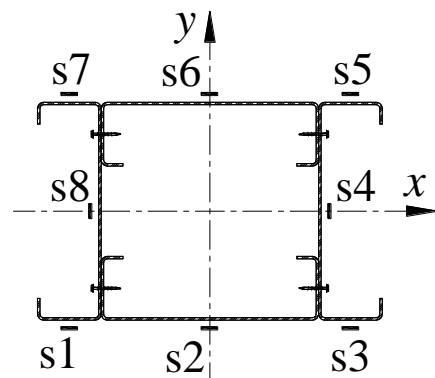


Fig. 3 Locations of strain gauges

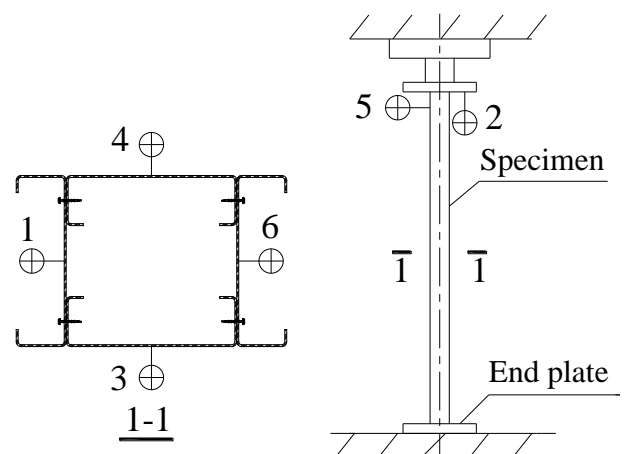


Fig. 4 Locations of displacement transducers (LVDTs)

along with the U-shaped track located at the both ends were directly placed in the test rig. Geometric alignment was conducted for all the specimens to guarantee the applied load being strictly axial.

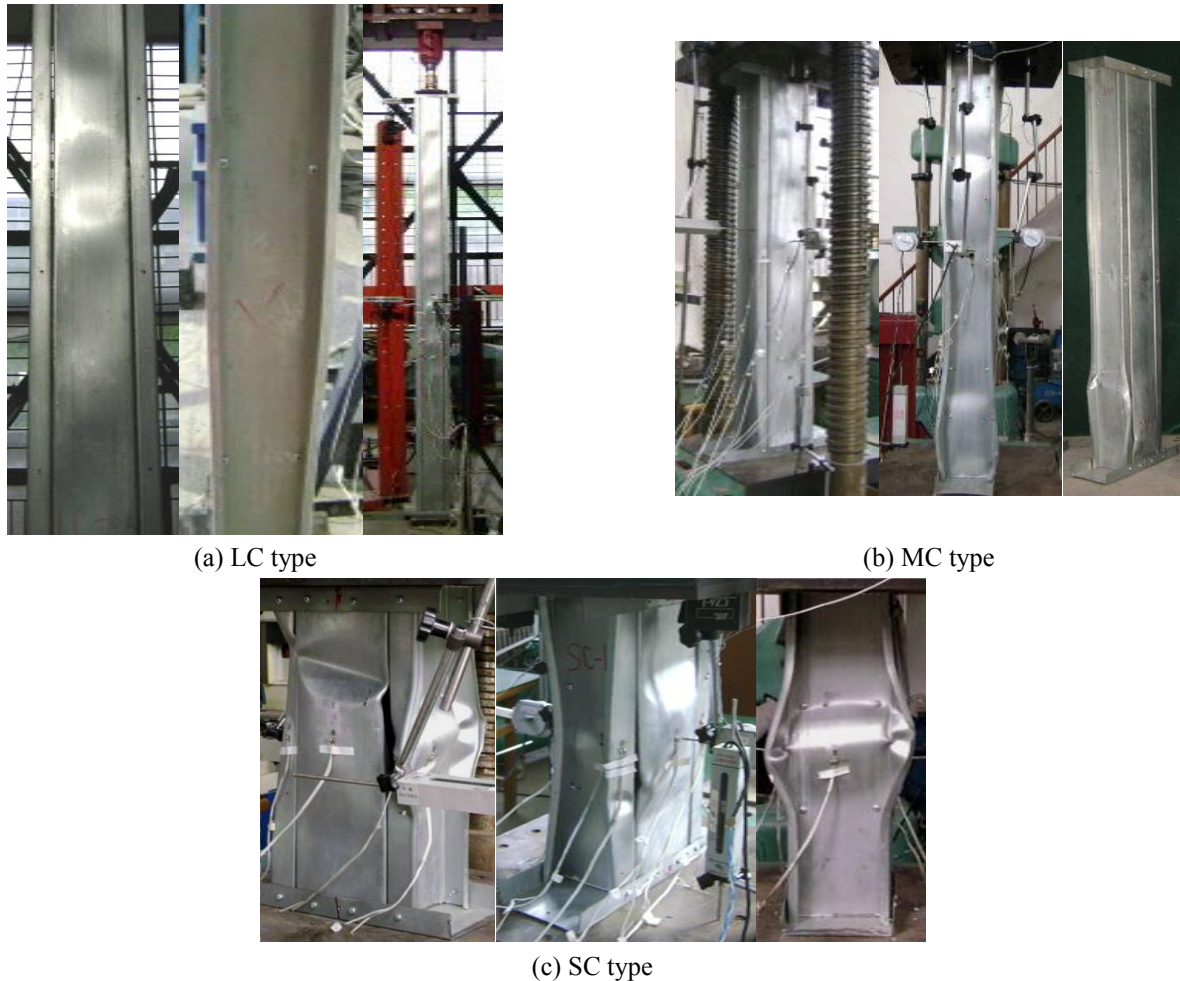


Fig. 5 Failure modes of the specimens

2.5 Measurement and loading protocol

Strain gauges were symmetrically mounted at the mid-height of the specimens, as shown in Fig. 3. Several linear variable differential transformers (LVDT) were mounted at the mid-height and the top of the specimens to measure the displacement of the relevant position on the column (see Fig. 4). The lateral displacements of the specimens were measured by LVDTs No.1,3,4 and 6, whereas the axial compressive displacements and the horizontal lateral displacements on the top of the specimens were measured by LVDTs No.2 and No.5, respectively. The load of each step was about 5% of the ultimate load lasting for 2 minutes, and then reading of the strain gauges and LVDTs were recorded. The load was applied continually until the load decreased to 85% of the ultimate load, then stop loading.

2.6 Test results

The test phenomena and failure modes were basically similar for all tests in this study: in the initial stage of loading, the built-up columns contacted with the U-shaped track located at both ends tightly. When the applied compressive load was raised to roughly 100kN, local buckling appeared on the webs of the column first, which

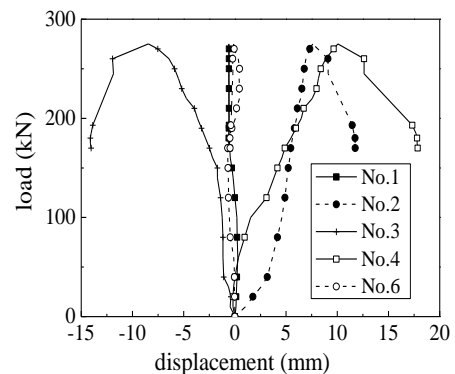


Fig. 6 Load-displacement curves for specimen SC-1

was followed by a development of distortional buckling at two external edges of the flanges and large compressive stresses in the post-buckling stage. It was shown that the eventual failure modes of the investigated three type specimens after the ultimate load were local and distortional buckling, as shown in Fig. 5.

The interaction between local and distortional buckling was obvious. Furthermore, it was shown during the test that each limb of the specimens could work together well when screw spacing ranging from 150mm to 300mm. No overall flexural buckling occurred for all columns in the test since

Table 2 Nominal dimensions, and comparisons between test results and design strengths of specimens

Specimen number	L^a (mm)	h^b (mm)	b_f^c (mm)	t^d (mm)	b_l^e (mm)	λ_x^f	λ_{xm}^g	P_T^h (kN)	P_A^i (kN)	P_{GB}^j (kN)	P_{DSM}^k (kN)	P_A/P_T	P_T/P_{GB}	P_T/P_{DSM}
LC-1	3000	140	41	1.6	14	52.6	34.2	270	277.72	266.67	276.15	1.03	1.01	0.98
LC-2	3000	140	41	1.6	14	52.6	34.2	220	277.72	266.67	276.15	1.26	0.83	0.80
MC-1	1200	140	41	1.6	14	21	13.7	270	292.66	276.79	287.62	1.08	0.98	0.94
MC-2	1200	140	41	1.6	14	21	13.7	290	292.66	276.79	287.62	1.01	1.05	1.01
MC-3	1200	140	41	1.6	14	21	13.7	280	292.66	276.79	287.62	1.05	1.01	0.97
SC-1	450	140	41	1.6	14	7.9	5.1	280	308.80	280.45	289.13	1.10	0.97	0.97
SC-2	450	140	41	1.6	14	7.9	5.1	315	308.80	280.45	289.13	0.98	1.12	1.09
SC-3	450	140	41	1.6	14	7.9	5.1	260	308.80	280.45	289.13	1.19	0.93	0.90

^a L is the nominal length of specimen;

^b h is the web height of C-shaped component;

^c b_f is the flange width;

^d t is the thickness;

^e b_l is the lip length;

^f λ_x is the slenderness ratio of built-up column around x -axis, if $K=1.0$, where K is the effective length factor;

^g λ_{xm} is the modified slenderness ratio of built-up column around x -axis, if $K=0.65$;

^h P_T is the ultimate strength of test;

ⁱ P_A is the ultimate strength obtained from ANSYS analysis;

^j P_{GB} is the ultimate strength obtained by GB50018-2002;

^k P_{DSM} is the ultimate strength obtained by direct strength method (DSM).

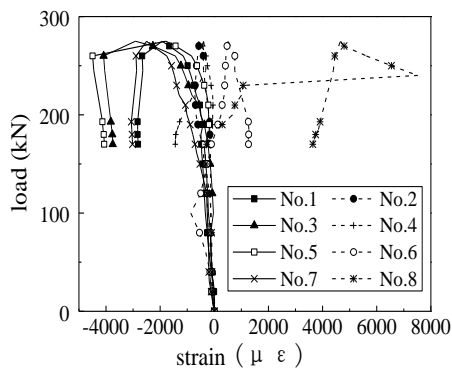


Fig. 7 Load-strain curves for specimen SC-1

the maximum slenderness ratio (λ_x) of all the specimens was controlled within 52.6. Thus, it is necessary to use numerical simulation method to analyze the axial compressive capacity of the quadruple C-channel built-up cold-formed steel columns with larger slenderness ratio in-depth. Finally, detailed test datum are given and summarized in Figs.6-7 and Table 2, where load-displacement and load-strain curves for specimen SC-1 is shown in Fig. 6 and Fig. 7, respectively.

3. Numerical simulation analysis

3.1 Finite element model

Numerical simulation analyses were conducted on the investigated quadruple C-channel built-up cold-formed steel columns using the nonlinear finite element software ANSYS. Initial geometric imperfections, nonlinear material

properties and contact problems of the columns were considered in the finite element models. The values of the initial imperfections of the columns were chosen as the first elastic buckling mode shape of the specimen subjected to the unit axial force, which was obtained by conducting the elastic buckling analysis on the investigated specimens in advance. With the relevant chosen amplitude, such an imperfection mode was subsequently incorporated in the nonlinear analysis of the columns. Based on the research results by Zhou (2007), the imperfection amplitude was taken as $0.0055b_w$ for local imperfection (b_w is the web width) herein. As for columns with larger slenderness ratio, the amplitude of expected geometric imperfection was selected as $L/750$ for global imperfection, where L was the length of column.

In the aspect of the modeling, the shell181 element was used for modeling the investigated cold-formed steel columns. Further, the solid45 elements were used to simulate the self-drilling screws, which was glued with the components together. The multi-linear kinematic hardening (MKIN) constitutive model of the material was considered in FEM. The values of the material parameters were determined according to the results obtained from the coupon tests, where the material's yield strength $f_y=334.04$ N/mm², Poisson's ratio $\nu=0.3$ and elastic modulus $E=2.23 \times 10^5$ N/mm². The stress and strain curves of the material in ANSYS analysis model in this study are shown in Fig. 8.

In order to simulate the boundary conditions of the columns appropriately, the displacements of all nodes along the x , y and z directions located on the bottom U-shaped track were constrained ($U_x=0$, $U_y=0$, $U_z=0$). Meanwhile, linear displacements of all nodes on the top U-shaped base in x and y directions were constrained ($U_x=0$, $U_y=0$).

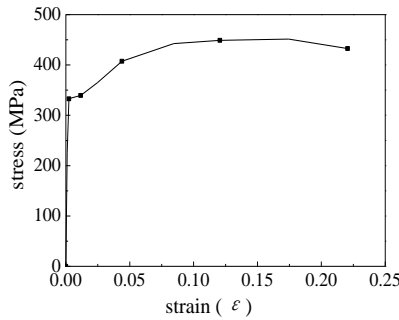
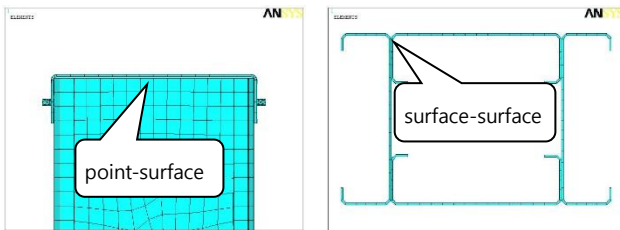


Fig. 8 Stress-strain curves of the material in ANSYS analysis model



(a) Point-surface contact (b) surface-surface contact

Fig. 9 Contacts in FEM model

Point-surface contact property was used to simulate the mechanical behavior between the specimen and U-shaped track. Whereas, “surface-surface” contact property was used for the interface for each limb of the C-shaped components (as shown in Fig. 9). The displacements in z -direction of all nodes on the top U-shaped track were coupled to a reference point. Then, the displacement was applied on this key point in z -direction.

It is worth to mention that a mesh sensitivity study was conducted in the numerical analysis for all columns to investigate the effect of the mesh size on the behavior of the specimens. It was shown that mesh sizes of $15\text{mm} \times 15\text{mm}$ for component part and $1\text{mm} \times 1\text{mm}$ for screw were appropriate, which can significantly reduce the computation time of the analysis with the validation of the numerical result being guaranteed. The typical finite element model of a quadruple C-channel built-up cold-formed steel column is shown in Fig. 10.

3.2 Validation of the numerical simulation results

The failure modes of the investigated columns with a Von Mises stress contour obtained from the numerical analyses are shown in Fig. 11. As it shown in Fig. 11, the failure modes of the columns in the finite element analysis (FEA) agreed well with the test results showed in Fig. 5, which proves the validation of the FEA conducted for the investigated columns. It is worth to mention that the obvious gaps were observed between four C-channel cold-formed steel components of the columns at the position where the maximum lateral deformation occurred (see Fig. 5), due to the absence of the relevant constraints at this position. On the contrary, four C-channel cold-formed steel components of the columns could work in harmony at positions having screw connections.

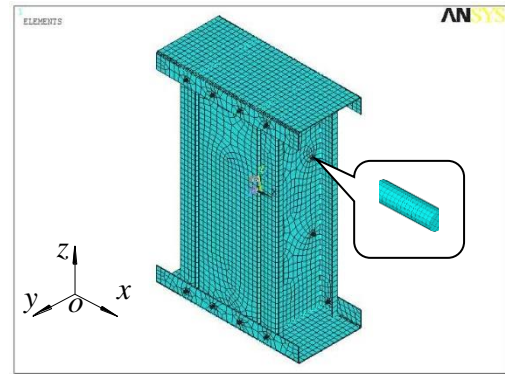


Fig. 10 The typical finite element model (for SC type specimen)

In the meantime, load-axial displacement curves of the investigated quadruple C-channel built-up cold-formed steel columns obtained from numerical analyses were compared with the test results, as shown in Fig. 12. The comparisons on axial compressive capacities between numerical analysis and the test results are summarized in Table 2. It was shown that the load-axial displacement curves and the maximum load in the FEA were in good agreement with that obtained from the tests (as shown in Fig. 12 and Table 2), which validated the accuracy of established FEM used for the further parametric analyses.

4. Parametric analyses

Based on the results obtained from the test and the verified numerical models, the parametric study was carried out to investigate the axial compressive structural behavior of quadruple C-channel built-up cold-formed steel columns in detail. The investigated parameters include the maximum slenderness ratio of the column, screw spacing and the flange width-to-thickness ratio, respectively. The columns were labeled so that the series and the column length could be identified easily. Taking the column, which labeled C140-t1.6-l3000-s300 as the example. The information which defines is given as follows:

“C140” indicates the web height of the C-shaped component is 140 mm.

“t1.6” indicates the thickness of C-shaped component is 1.6 mm.

“l3000” indicates the column specimen length is 3000 mm.

“s300” indicates the screw spacing is 300 mm.

4.1 Influence of the slenderness ratio

FEM models for columns with different lengths were designed to study the influence of maximum slenderness ratio of the column. The investigated lengths of columns include $l=450\text{mm}$, 1200mm , 2100mm , 3000mm , 4200mm , 5100mm , 6000mm , 6900mm , 7800mm , 8700mm .

The screw spacing of the short columns was 150mm while that for the long columns was 300mm . The numerical analysis results are summarized in Table 3. The load-axial displacement relationships of columns with different length

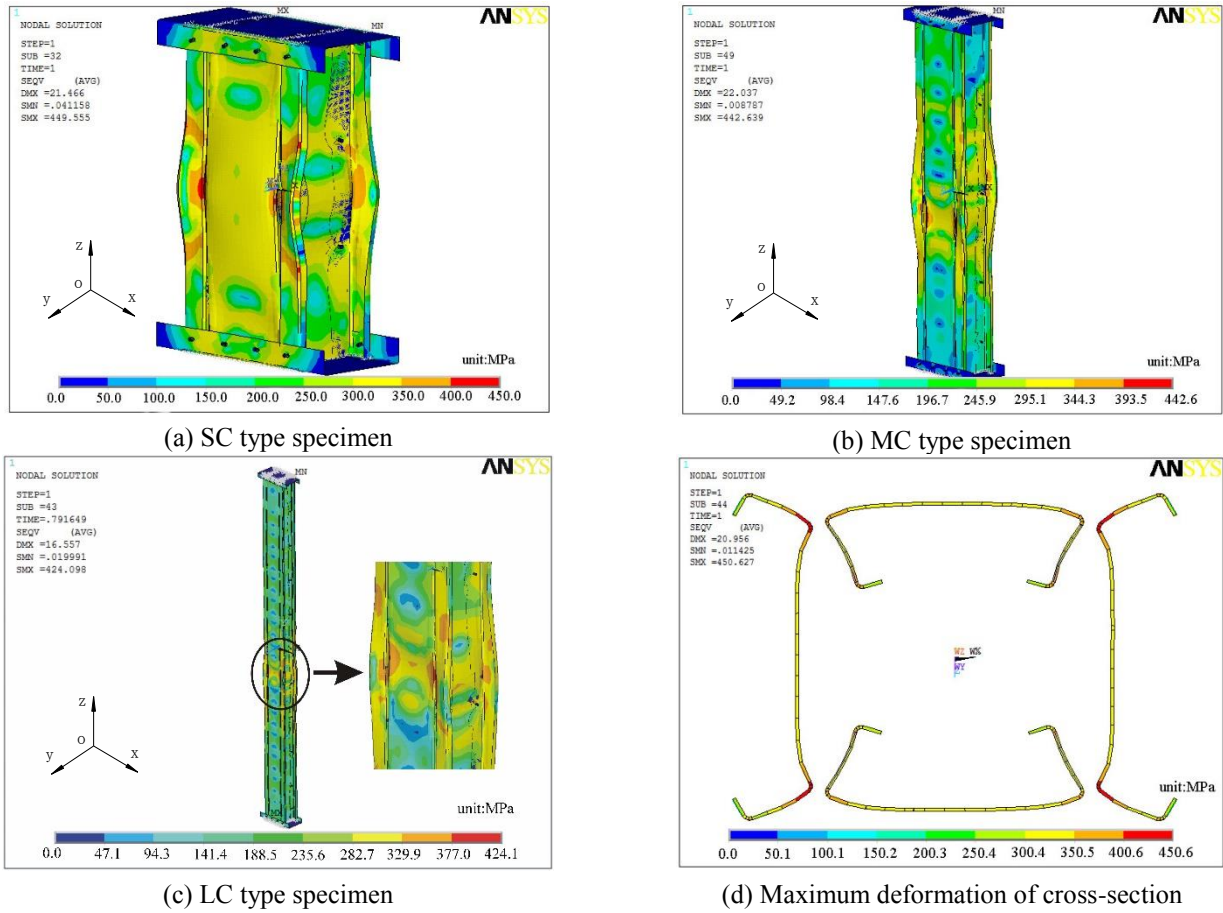


Fig. 11 Von Mises stress contour and failure modes of specimens obtained from ANSYS analyses

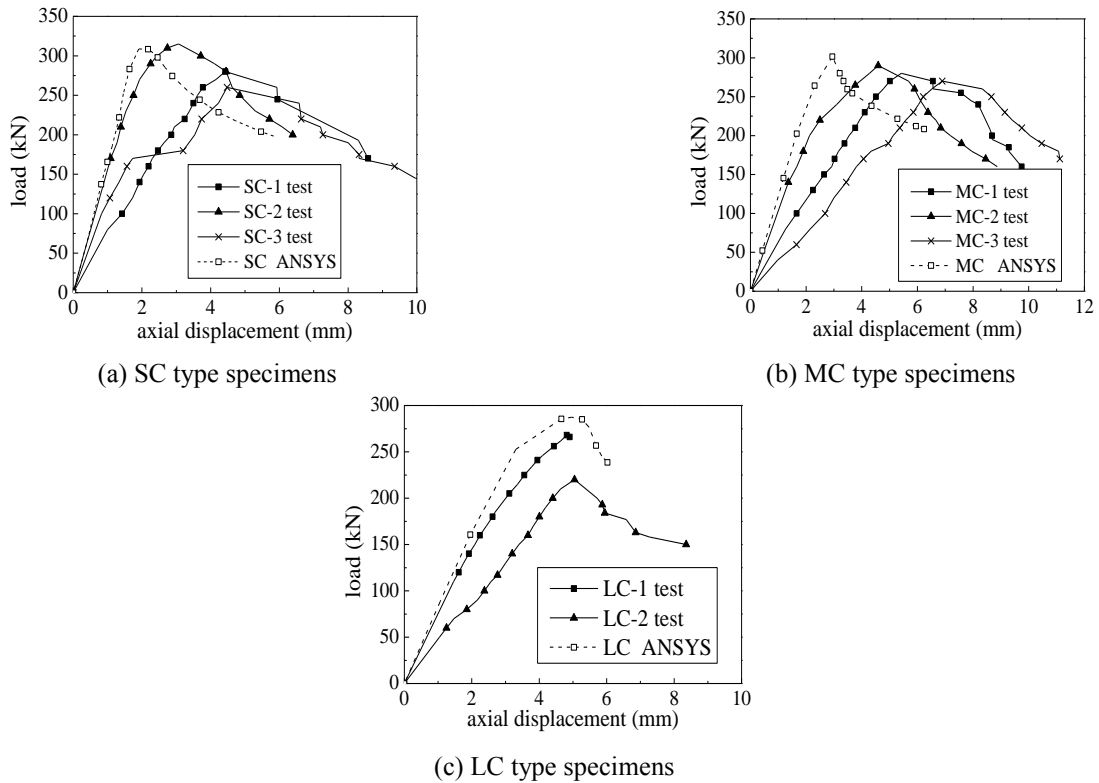


Fig. 12 Comparison of load-axial displacement curves

Table 3 Comparisons between the investigated design methods

specimen	λ_x	λ_{xm}	P_A (kN)	P_{GB} (kN)	P_{DSM} (kN)	P_A/P_{GB}	P_A/P_{DSM}	Failure mode
C140-t1.6-l450-s150	7.9	5.1	308.80	280.45	289.14	1.101	1.068	
C140-t1.6-l1200-s300	21	13.7	292.66	276.79	287.62	1.057	1.018	
C140-t1.6-l2100-s300	36.8	23.9	286.83	272.09	283.06	1.054	1.013	L ^a + D ^b
C140-t1.6-l3000-s300	52.6	34.2	277.72	266.67	276.15	1.041	1.006	
C140-t1.6-l4200-s300	71	46.2	271.91	258.8	263.58	1.051	1.032	
C140-t1.6-l5100-s300	89.4	58.1	260.39	251.65	251.92	1.035	1.034	
C140-t1.6-l6000-s300	105.2	68.4	255.47	242.14	238.63	1.055	1.071	
C140-t1.6-l6900-s300	121	78.7	247.38	228.02	224.02	1.085	1.104	F ^c
C140-t1.6-l7800-s300	136.7	88.9	235.2	207.03	208.39	1.136	1.129	
C140-t1.6-l8700-s300	152.5	99.1	225.2	185.86	192.06	1.212	1.173	
C89-t1.0-l450-s150	13	8.4	168.28	126.95	142.23	1.326	1.183	
C89-t1.0-l1200-s300	34.6	22.5	149.15	124.2	139.74	1.201	1.067	
C89-t1.0-l2400-s300	71	46.1	138.04	118.8	131.39	1.162	1.051	L ^a + D ^b
C89-t1.0-l3000-s300	86.5	56.2	134.73	115.5	125.44	1.166	1.074	
C89-t1.0-l4200-s300	121	78.7	125.49	104.78	110.78	1.198	1.133	F ^c
C89-t1.0-l5100-s300	147.1	95.6	120.59	91.97	98.13	1.311	1.229	
C89-t1.6-l300-s150	8.7	5.6	321.21	284.92	301.98	1.127	1.064	
C89-t1.6-l450-s300	13	8.4	301.51	283.22	301.47	1.065	1.000	
C89-t1.6-l1200-s300	34.6	22.5	287.15	274.33	295.89	1.047	0.970	L ^a + D ^b
C89-t1.6-l1800-s300	51.9	33.7	278.81	266.12	287.95	1.048	0.968	
C89-t1.6-l2400-s300	71	46.1	267.56	257.11	277.15	1.041	0.965	
C89-t1.6-l3000-s300	86.5	56.2	261.11	247.03	263.82	1.057	0.990	
C89-t1.6-l3600-s300	103.8	67.5	252.83	233.38	248.32	1.083	1.018	
C89-t1.6-l4200-s300	121	78.7	245.49	215.99	229.29	1.137	1.071	F ^c
C89-t1.6-l5100-s300	147.1	95.6	220.2	182.73	190.22	1.205	1.158	

^aL=Local buckling

^bD=Distortional buckling

^cF=Flexural buckling.

are illustrated in Fig. 13. The influences of slenderness ratio on the axial compressive capacity of columns are shown in Fig. 14. As shown in Fig. 14, λ_x is the slenderness ratio of built-up column around x -axis, as K is assumed to be 1.0, where K is the effective length factor.

According to Table 3, Figs.13-14, the results show that the slenderness ratio have a remarkable influence on the axial compressive behavior of the quadruple C-channel built-up cold-formed steel columns, where the ultimate compressive capacity and stiffness of columns decrease with the increase of the slenderness ratio. On the other hand, the failure modes of columns vary according to the slenderness ratio of the column being assessed. The failure modes of columns with a small slenderness ratio (as for C140-t1.6 type columns, if $\lambda_x < 71$; as for C89 type columns, if $\lambda_x < 86.5$) are local and distortional buckling, whereas the failure mode of columns with large slenderness ratio is overall flexural buckling.

4.2 Influence of the screw spacing

FEM models for columns with different lengths were designed to study the influence of screw spacing on the specimens further. In this section, the columns were divided into four groups according to the specimens' length: 900mm, 2700 mm, 4500mm and 6300 mm. The corresponding self-drilling screw spacing of the columns in group was 150 mm, 300 mm and 450 mm, respectively. The load-axial displacement curves obtained from numerical analyses for the above specimens are illustrated in Fig. 15. The other numerical analytical results for the above specimens are summarized in Table 4.

According to the analytical results of Table 4 and Fig. 15, it can be found that screw spacing ranging from 150mm to 450mm has less impact on the axial compressive capacity of columns in the same group. When the columns are in the same group, the difference of axial compressive capacity from each other is within 5%.

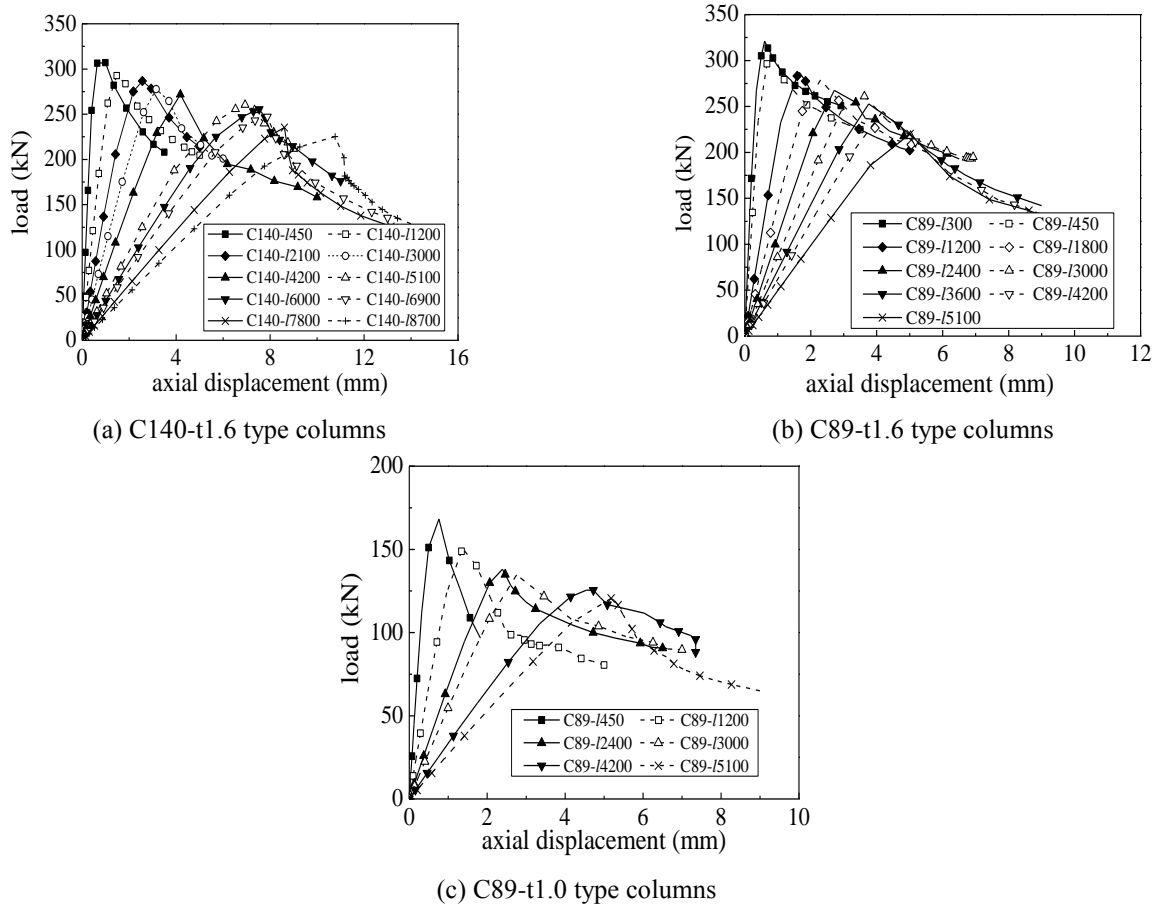


Fig. 13 Load-axial displacement curves of columns with different length

Table 4 Influences of self-drilling screw spacing

Specimen	s^a (mm)	P_A (kN)	Specimen	s^a (mm)	P_A (kN)
C140-t1.6-l900-s150	150	300.37	C140-t1.6-l4500-s150	150	278.57
C140-t1.6-l900-s300	300	293.60	C140-t1.6-l4500-s300	300	265.44
C140-t1.6-l900-s450	450	292.12	C140-t1.6-l4500-s450	450	264.71
C140-t1.6-l2700-s150	150	288.90	C140-t1.6-l6300-s150	150	250.19
C140-t1.6-l2700-s300	300	280.97	C140-t1.6-l6300-s300	300	248.10
C140-t1.6-l2700-s450	450	277.16	C140-t1.6-l6300-s450	450	242.38

^a s is the screw spacing

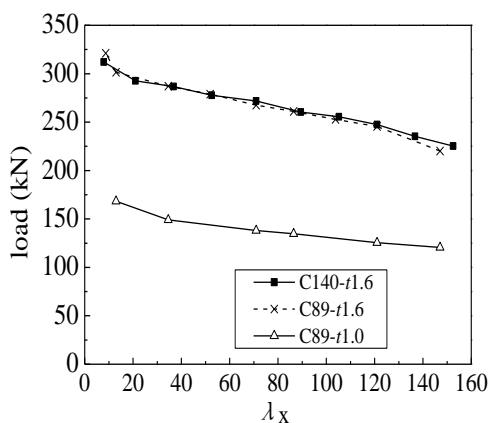


Fig. 14 Influences of slenderness ratio on axial compressive bearing capacity of columns

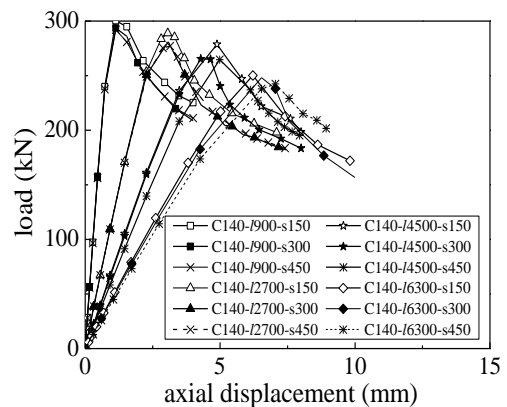


Fig. 15 Load-axial displacement curves of columns with different screw spacing

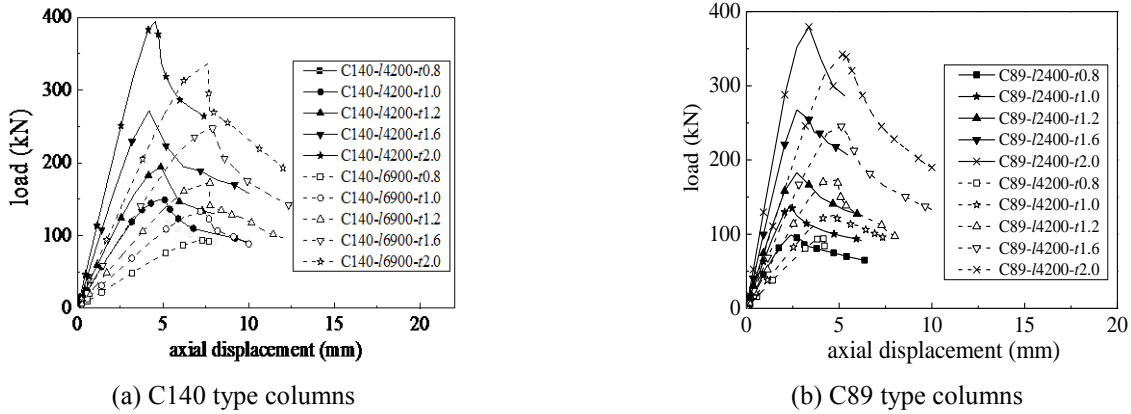


Fig. 16 Load-axial displacement curves of columns with different thickness

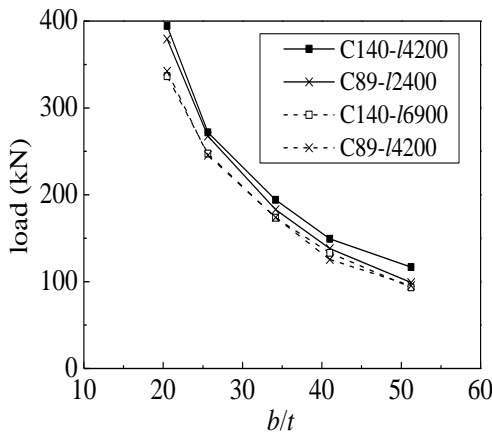


Fig. 17 Influence curves of the flange width-to-thickness ratio on the axial compressive capacity of columns

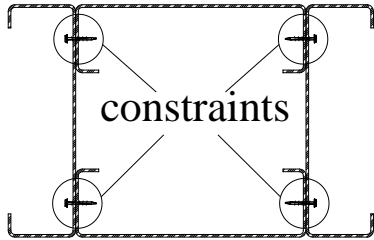


Fig. 18 Locations of the constraints

4.3 Influence of flange width-to-thickness ratio

The influence of the flange width-to-thickness ratio on the axial compressive capacity of columns was analyzed in this section. The screw spacing of 300mm and the flange width of 41mm were maintained in the investigated C140 and C89 type columns. Columns were divided into five groups according to the thickness of the component, where the investigated component thickness includes 0.8 mm, 1.0 mm, 1.2 mm, 1.6 mm and 2.0 mm, respectively. The corresponding numerical analysis results are summarized in Table 5. The load-axial displacement relationships of columns with different thickness are shown in Fig. 16. The influence curves of the flange width-to-thickness ratio on the axial compressive capacity of columns are shown in Fig. 17.

The results in Table 5, Figs.16-17 indicate that the flange width-to-thickness ratio has a significant impact on the axial compressive capacity of columns: the axial compressive capacity of all columns decrease significantly when the flange width-to-thickness ratio changes from 20.5 to 51.25. Therefore, the mechanical behavior of the specimen could be improved by the decrease of the flange width-to-thickness ratio, since such method can significantly improve the buckling stability of the built-up columns.

5. Design rules

In this section, two commonly used design methods, namely the effective ratio of width-to-thickness method in section 5.1 of the Chinese code (GB50018 2002) and the direct strength method (DSM) (AISI 2007) in section 5.2, for cold-formed steel columns were briefly reviewed. It should be noted that none of these two methods cover the contents for designing the quadruple C-channel built-up cold-formed steel columns. For this reason, the validation and appropriation of these two methods for the quadruple C-channel built-up cold-formed steel columns in this study were investigated in section 5.3.

5.1 Effective ratio of width to thickness method

According to GB50018 (2002), axial compressive capacity of columns is given by

$$P_{GB} = \varphi A_e f_y \tag{1}$$

where φ represents the overall stability coefficient which can be calculated by Eq. (2), A_e is the effective cross-sectional area of the column, f_y is the yield stress.

$$\varphi = \left[1 + (1 + \varepsilon_0) / \bar{\lambda}^2 \right] / 2 - \sqrt{\left[1 + (1 + \varepsilon_0) / \bar{\lambda}^2 \right]^2 / 4 - 1 / \bar{\lambda}^2} \tag{2}$$

where ε_0 is the equivalent eccentricity. For Q235 steel, it can be calculated by Eq. (3).

$$\varepsilon_0 = \begin{cases} \bar{\lambda} \leq 0.5 & \varepsilon_0 = 0.25\bar{\lambda} \\ 0.5 < \bar{\lambda} \leq 1.0 & \varepsilon_0 = 0.05 + 0.15\bar{\lambda} \\ \bar{\lambda} \geq 1.0 & \varepsilon_0 = 0.05 + 0.15\bar{\lambda}^2 \end{cases} \tag{3}$$

Table 5 Influences of flange width-to-thickness ratio

Specimen	b_f (mm)	t (mm)	b_f/t	P_A (kN)	Specimen	b_f (mm)	t (mm)	b_f/t	P_A (kN)
C140-t0.8-l4200-s300	41	0.8	51.25	116.83	C140-t0.8-l6900-s300	41	0.8	51.25	93.46
C140-t1.0-l4200-s300	41	1.0	41	149.24	C140-t1.0-l6900-s300	41	1.0	41	133.12
C140-t1.2-l4200-s300	41	1.2	34	194.06	C140-t1.2-l6900-s300	41	1.2	34	173.44
C140-t1.6-l4200-s300	41	1.6	25.6	271.91	C140-t1.6-l6900-s300	41	1.6	25.6	247.38
C140-t2.0-l4200-s300	41	2.0	20.5	394.43	C140-t2.0-l6900-s300	41	2.0	20.5	336.48
C89-t0.8-l2400-s300	41	0.8	51.25	99.03	C89-t0.8-l4200-s300	41	0.8	51.25	95.34
C89-t1.0-l2400-s300	41	1.0	41	138.04	C89-t1.0-l4200-s300	41	1.0	41	125.49
C89-t1.2-l2400-s300	41	1.2	34	182.98	C89-t1.2-l4200-s300	41	1.2	34	173.85
C89-t1.6-l2400-s300	41	1.6	25.6	267.56	C89-t1.6-l4200-s300	41	1.6	25.6	245.49
C89-t2.0-l2400-s300	41	2.0	20.5	379.35	C89-t2.0-l4200-s300	41	2.0	20.5	342.26

where $\bar{\lambda} = \sqrt{\frac{f_y}{\sigma_E}} = \frac{\lambda}{\pi} \sqrt{\frac{f_y}{E}}$, E is the Young's modulus of the steel, σ_E is the Euler buckling stress, λ is the overall slenderness ratio of the whole cross-section with respect to the built-up member axis, which can be calculated by Eq. (4).

$$\lambda = \left(\frac{KL}{r} \right) \quad (4)$$

where K is the effective length factor and is proposed to be a constant value of 0.65 taking the U-shaped track conditions into the consideration as recommended by Miller and Pekoz (1993); L is the nominal length of member, r is the radius of gyration of full unreduced cross section with respect to the axis of buckling.

The effective width is given by

$$\begin{cases} \frac{b_c}{t} = \frac{b_c}{t} & \text{if } \frac{b}{t} \leq 18\alpha\rho \\ \frac{b_c}{t} = \left(\sqrt{\frac{21.8\alpha\rho}{b/t}} - 0.1 \right) \frac{b_c}{t} & \text{if } 18\alpha\rho < \frac{b}{t} < 38\alpha\rho \\ \frac{b_c}{t} = \frac{25\alpha\rho}{b/t} \frac{b_c}{t} & \text{if } \frac{b}{t} \geq 38\alpha\rho \end{cases} \quad (5)$$

where b is the width of the plate, t is the thickness of the plate, b_c is the effective width of the plate, α is the calculating coefficient, $\alpha=1.15-0.15\psi$ and $\alpha=1.15$ if $\psi < 0$, ψ is the stress distribution uniformity coefficient, b_c is the width of compressive zone; $\rho = \sqrt{205k_1k/\sigma_1}$, k_1 is the restraining coefficient of the plates, k is the compressive stability coefficient of the plates, $\sigma_1 = \varphi f_y$. In order to compare it with the test results, $\rho = \sqrt{205k_1k/\sigma_1}$ in this paper.

5.2 Direct strength method

The direct strength method (DSM) has the advantage of simplicity in designing the structural members with complicated sectional configurations. The design rules of the DSM for columns in the North American Specification (AISI 2007) are given as follows:

$$P_{DSM} = \min(P_{ne}, P_{nl}, P_{nd}) \quad (6)$$

where P_{ne} , P_{nl} , P_{nd} represent the nominal axial strength for overall buckling load, local buckling load and distortional buckling, respectively. P_{ne} , P_{nl} , P_{nd} are given by Eqs. (7) - (9).

$$\begin{cases} \lambda_c \leq 1.5 & P_{ne} = \left(0.658 \lambda_c^2 \right) P_y \\ \lambda_c > 1.5 & P_{ne} = \left(\frac{0.877}{\lambda_c^2} \right) P_y \end{cases} \quad (7)$$

Where $\lambda_c = \sqrt{P_y/P_{cre}}$, $P_y = Af_y$, $P_{cre} = Af_{cre}$, P_{cre} is the critical elastic overall buckling load, f_{cre} is the elastic overall buckling stress.

$$\begin{cases} \lambda_1 \leq 0.776 & P_{nl} = P_{ne} \\ \lambda_1 > 0.776 & P_{nl} = \left[1 - 0.15 \left(\frac{P_{crl}}{P_{ne}} \right)^{0.4} \right] \left(\frac{P_{crl}}{P_{ne}} \right)^{0.4} P_{ne} \end{cases} \quad (8)$$

Where $\lambda_1 = \sqrt{P_{ne}/P_{crl}}$, $P_{crl} = Af_{crl}$, P_{crl} is the critical elastic local buckling load, f_{crl} is the elastic local buckling stress.

$$\begin{cases} \lambda_d \leq 0.561 & P_{nd} = P_{ne} \\ \lambda_d > 0.561 & P_{nd} = \left[1 - 0.25 \left(\frac{P_{crl}}{P_{ne}} \right)^{0.6} \right] \left(\frac{P_{crl}}{P_{ne}} \right)^{0.6} P_{ne} \end{cases} \quad (9)$$

Where $\lambda_d = \sqrt{P_y/P_{crl}}$, $P_{crl} = Af_{crl}$, P_{crl} is the critical elastic distortional buckling load, f_{crl} is the elastic distortional buckling stress.

The f_{cre} , f_{crl} and f_{crl} in Eqs. (7) - (9) were obtained by the software CUFSM (Schafer 2012) with the following assumption as shown in Fig. 18, where the locations of screws were set as constraints in the software CUFSM.

It should be noted that, when calculating the f_{cre} in above Eqs. (6)-(9), the modified slenderness ratio specified by AISI (2007) was not adopted. Because the modified slenderness ratio, which is based on the researches of hot-rolled built-up members (Zandonini 1985, Aslani and Goel

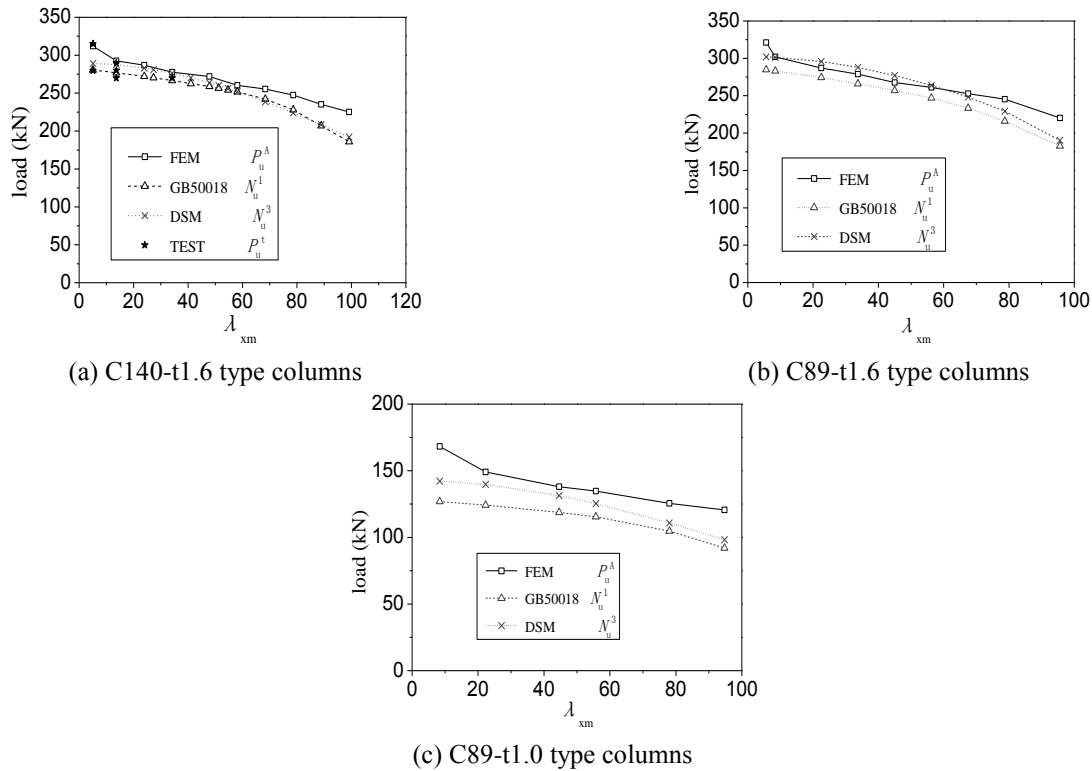


Fig. 19 Comparison of FEA, test results and design strengths

1991), is not suitable for complex built-up cold-formed steel columns due to the small distance between individual members as illustrated by Li *et al.* (2014). Furthermore, the end support condition is between hinged and fixed, which is like the ends in the study by Miller and Pekoz (1993). Thus, the effective length factor K is assumed to be 0.65 based on the research results obtained from Miller and Pekoz (1993) in this paper.

5.3 Comparison of numerical and test results with design predictions

The column strengths obtained from the test specimens (P_t) and the FEA (P_A) were compared with the design strengths (P_{GB} , P_{DSM}), as shown in Tables 2-3 and Fig. 19. Meanwhile, λ_{xm} is the modified slenderness ratio of built-up column around x -axis which can be calculated by Eq. (4).

It can be found that the design strengths P_{GB} obtained by the effective ratio of the width-to-thickness method in GB50018 and P_{DSM} obtained from DSM, assuming the effective length factor K is 0.65, are generally safer than the strength P_A obtained from the FEA. But for the column type C89-t1.6, P_{DSM} are unsafe if $10 < \lambda_{xm} < 60$. The difference between P_A and P_{DSM} is within 4%. Thus, it is suitable to assume effective length factor K as 0.65 for quadruple C-channel built-up cold-formed steel columns with U-shaped base in the ends.

6. Conclusions

In this study, the axial compressive behavior of novel quadruple C-channel built-up cold-formed steel columns

with different slenderness ratio were investigated using the experimental and numerical analysis. The stiffness and axial compressive capacity of the columns were analyzed. Some conclusions can be drawn as follows:

- The investigated quadruple C-channel built-up cold-formed steel columns show obvious post-buckling strength. The interaction between local and distortional buckling is obvious. The failure modes of columns are local and distortional buckling due to the small slenderness ratio in the tests.
- The numerical simulation results for the axial compressive capacity of the built-up columns agree well with the test results, which verifies the rationality and accuracy of the FE analysis.
- The structural behavior of the columns is significantly affected by the maximum slenderness ratio. The axial compressive capacity and stiffness of the quadruple C-channel built-up cold-formed steel columns decreases obviously with the increase of the maximum slenderness ratio. When the screw spacing ranges from 150mm to 450mm, the axial compressive capacity and stiffness of the quadruple C-channel built-up cold-formed steel columns change little. The screw spacing in 150mm-300mm is reasonable, and each component of the column could work together well. The axial compressive capacity of quadruple C-channel built-up cold-formed steel columns increases with the decrease of the flange width-thickness ratio. Meanwhile, the deformation could be postponed and the mechanical behavior could be improved.
- The design strengths P_{GB} obtained by the effective ratio of the width-to-thickness method in GB50018 and P_{DSM} obtained from DSM, assuming the effective length

factor K is 0.65, are generally safer than the strength P_A obtained from the FEA. It is suitable to assume the effective length factor K as 0.65 for quadruple C-channel built-up cold-formed steel columns with U-shaped base in the ends.

Acknowledgements

In this paper, the research work was supported by the National Natural Science Foundation of China (No.51878055), the key Research and Development Program of Shaanxi Province(2018SF-354) and Fundamental Research Funds for the Central Universities, CHD (300102289205).

References

- Anbarasu, M., Kumar, S.B. and Sukumar, S. (2013), "Study on the effect of ties in the intermediate length Cold Formed Steel (CFS) columns", *Struct. Eng. Mech.*, **46** (3), 323-335. <https://doi.org/10.12989/sem.2013.46.3.323>.
- Anbarasu, M. and Sukumar, S. (2014), "Influence of spacers on ultimate strength of intermediate length thin walled columns", *Steel Compos. Struct.*, **16**(4), 437-454. <https://doi.org/10.12989/scs.2014.16.4.437>.
- AISI (2007), North American specification for the design of cold-formed steel structural members, Washington, DC, USA.
- Aslani, F. and Goel, S.C. (1991), "An analytical criterion for buckling strength of built-up compression members", *Eng. J. AISC*, **28**(4), 159-168.
- AS/NZS No. 4600 (2005), Cold-formed Steel Structure, Sydney, Australia.
- Biggs, K.A., Ramseyer, C., Ree, S. and Kang, T.H.K. (2015), "Experimental testing of cold-formed built-up members in pure compression", *Steel Compos. Struct.*, **18**(6), 1331-1351. <https://doi.org/10.12989/scs.2015.18.6.1331>.
- Dabaon, M., Ellobody, E. and Ramzy, K. (2015), "Experimental investigation of built-up cold-formed steel section battened columns", *Thin-Walled Struct.*, **92**, 137-145. <https://doi.org/10.1016/j.tws.2015.03.001>.
- Dong, J., Wang, S.Q. and Lu, X. (2006), "Simulations of the hysteretic behavior of thin-wall cold-formed steel members under cyclic uniaxial loading", *Struct. Eng. Mech.*, **24**(3), 323-337. <https://doi.org/10.12989/sem.2006.24.3.323>.
- Eurocode 3 (2006), Design of steel structures—Part 1-3: General rules supplementary rules for cold-formed members and sheeting, BS EN 1993-1-3, Brussels.
- Georgieva, I., Schueremans, L. and Pyl, L. (2012), "Composed columns from cold-formed steel Z-profiles: Experiments and code-based predictions of the overall compression capacity", *Eng. Struct.*, **37**(4), 125-134. <https://doi.org/10.1016/j.engstruct.2011.12.017>.
- GB50018 (2002), Technical Code of Cold-formed Thin-wall Steel Structures, Beijing, China.
- GB/T228.1 (2010), Metallic materials: Tensile testing: part 1: Method of test at room temperature, Beijing, China.
- Heva, Y.B. and Mahendran, M. (2013), "Flexural-torsional buckling tests of cold-formed steel compression members at elevated temperatures", *Steel Compos. Struct.*, **14**(3), 205-227. <https://doi.org/10.12989/scs.2013.14.3.205>.
- Kripka, M. and Pravia, Z.M.C. (2013), "Cold-formed steel channel columns optimization with simulated annealing method", *Struct. Eng. Mech.*, **48**(3), 383-394. <https://doi.org/10.12989/sem.2013.48.3.383>.
- Li, Y.Q., Li, Y.L., Wang, S.K. and Shen, Y.Z. (2014), "Ultimate load-carrying capacity of cold-formed thin-walled columns with built-up box and I section under axial compression", *Thin-Walled Struct.*, **79**(3), 202-217. <https://doi.org/10.1016/j.tws.2014.02.003>.
- Miller, T.H. and Pekoz, T. (1993), "Behavior of cold-formed steel wall stub assemblies", *J. Struct. Eng.*, **119**(2) 641-651.
- Muthuraj, H., Sekar, S.K., Mahendran, M. and Deepak, O.P. (2017), "Post buckling mechanics and strength of cold-formed steel columns exhibiting Local-Distortional interaction mode failure", *Struct. Eng. Mech.*, **64**(5), 621-640. <https://doi.org/10.12989/sem.2017.64.5.621>.
- Peters, G.K. (2003), "An investigation of the effects of fastener spacing in build-up cold-formed steel compression members", M.Sc. Dissertation, University of Dalhousie, Canada.
- Piyawat, K., Ramseyer, C. and Kang, T.H.K. (2013), "Development of an Axial Load Capacity Equation for Doubly-Symmetric Built-Up Cold-Formed Sections," *J. Struct. Eng.*, **139**(12), 04013008.
- Schafer, B.W. (2012), CUFSM4.05: Finite strip buckling analysis of thin-walled members, Johns Hopkins University, Baltimore, U.S.A. <http://www.ce.jhu.edu/bschafer/cufsm>.
- Stone, T.A. and La Boube, R.A. (2005), "Behavior of cold-formed steel built-up I-sections", *Thin-Walled Struct.*, **43**(12), 1805-1817. <https://doi.org/10.1016/j.tws.2005.09.001>.
- Whittle, J. and Ramseyer, C. (2009), "Buckling capacities of axially loaded, cold-formed, built-up C-channels", *Thin-Walled Struct.*, **47**(2), 190-201. <https://doi.org/10.1016/j.tws.2008.05.014>.
- Young, B. and Chen, J. (2008), "Column tests of cold-formed steel non-symmetric lipped angle sections", *J. Constr. Steel Res.*, **64**(7), 808-815. <https://doi.org/10.1016/j.jcsr.2008.01.021>.
- Young, B. and Rasmussen, K.J.R. (1998), "Tests of fixed-ended plain channel columns", *J. Struct. Eng.*, **124**(2), 131-139.
- Yu, W.W. (2000), *Cold Formed Steel Design*, 3rd Edition, John Wiley & Sons Inc., New York, NY, USA.
- Zandonini, R. (1985), "Stability of compact built-up struts: experimental investigation and numerical simulation", *Constr. Met.*, **4**, 288.
- Zhang, J.H. and Young, B. (2015), "Numerical investigation and design of cold-formed steel built-up open section columns with longitudinal stiffeners", *Thin-Walled Struct.*, **89**, 178-191. <https://doi.org/10.1016/j.tws.2014.12.011>.
- Zhou, L.H. (2007), "Experimental and theoretical research on high strength cold-formed thin-walled steel stub columns under compression", M.Sc. Dissertation, Chang'an University, China.
- Zhou, W.B. and Jiang, L.Z. (2017), "Distortional buckling of cold-formed lipped channel columns subjected to axial compression", *Steel Compos. Struct.*, **23**(3), 331-338. <http://doi.org/10.12989/scs.2017.23.3.331>.

CC